

Photoionization mass spectrometry of CH₂S and HCS

B. Ruscic and J. Berkowitz

Chemistry Division, Argonne National Laboratory, Argonne, Illinois 60439

(Received 4 August 1992; accepted 19 October 1992)

The transient species CH₂S and HCS were studied by photoionization mass spectrometry. They were prepared *in situ* from CH₃SH by sequential hydrogen abstraction with fluorine atoms. CH₂S was also prepared by pyrolysis of CH₃SCl and CH₃SSCH₃. The photoion yield curve of CH₂S displays an abrupt threshold, and is similar in overall shape to that of the homologue CH₂O. The adiabatic ionization potential of CH₂S is found to be 9.376 ± 0.003 eV. Evidence has been found for *nd* and/or *ns* and *np* Rydberg states converging to the first excited state of CH₂S⁺. In addition, the HCS⁺ fragment from CH₂S has been determined to appear at <11.533 ± 0.021 eV at 0 K. In contrast to CH₂S, the photoion yield curve of HCS⁺ from HCS displays a very broad Franck–Condon envelope, consistent with a transition from bent HCS to linear HCS⁺. A Poisson fit to the experimental Franck–Condon factors indicates that the adiabatic ionization potential of HCS is <7.499 ± 0.005 eV, and perhaps as low as 7.412 ± 0.007 eV. The fragment curves at *m/e* = 46, 47, 48, and 49 from CH₃SSCH₃ have also been examined, and their relative shifts in energy determined. Together with measurements on CH₂S and HCS, and the previously reported Δ*H*_{*f*0}^o(CH₂SH⁺) = 211.5 ± 2.0 kcal/mol (<213.1 ± 0.2 kcal/mol), this is sufficient to establish Δ*H*_{*f*0}^o(CH₂S) = 28.3 ± 2.0 kcal/mol (<29.9 ± 0.9 kcal/mol) and Δ*H*_{*f*0}^o(HCS) = 71.7 ± 2.0 kcal/mol (<73.3 ± 1.0 kcal/mol), >69.7 ± 2.0 kcal/mol). These values are in very good agreement with recent *ab initio* calculations. The implications for various bond energies within the CH_{*n*}S system are also discussed.

I. INTRODUCTION

In the course of recent photoionization mass spectrometric (PIMS) studies¹ of CH₂SH and CH₃S produced by the reaction of F atoms with CH₃SH, we noted that measurable quantities of CH₂S and HCS were being generated, presumably by successive H atom abstraction. Two prior photoelectron spectroscopic studies of CH₂S have been reported. Kroto and Suffolk² obtained 9.34 ± 0.01 eV for the adiabatic ionization potential (I.P.) of CH₂S, while the experiments of Solouki *et al.*³ yielded 9.38 eV. We are unaware of any previous studies on the HCS species. Thus an examination of HCS and CH₂S by PIMS seemed in order.

An indirect approach to I.P.(HCS) is possible if both Δ*H*_{*f*0}^o(HCS⁺) and Δ*H*_{*f*0}^o(HCS) are well known. Butler and Baer⁴ had determined appearance potentials (A.P.) of HCS⁺ from thiirane (C₂H₄S), thietane (C₃H₆S), tetrahydrothiophene (C₄H₈S) and thiophene (C₄H₄S). From the experiments with thietane and tetrahydrothiophene, they deduced Δ*H*_{*f*0}^o(HCS⁺) = 233 ± 2 kcal/mol. The high value obtained from thiirane (245 ± 2 kcal/mol) was attributed to a reverse activation barrier, while that from thiophene (<251 ± 2 kcal/mol) was considered to be affected by a kinetic shift, since C₂H₂S⁺ appeared at a lower energy. Earlier, Butler and Baer⁵ had determined Δ*H*_{*f*298}^o(HCS) < 73 ± 2 kcal/mol; combining these values leads to I.P.(HCS) > 6.9 ± 0.1 eV. More recently, the proton affinity (P.A.) of CS has been measured by Smith and Adams⁶ to be 188.2 ± 1 kcal/mol, and calculated by Botschwina and Sebald⁷ to be 189.5 ± 1.2 kcal/mol. These values, together with Δ*H*_{*f*0}^o(CS) = 65.9 ± 0.5 kcal/mol (Ref. 8) [or 65.6 ± 0.3 kcal/mol (Ref. 9)] yield

Δ*H*_{*f*0}^o(HCS⁺) = 243.9 ± 1.2 kcal/mol (Ref. 6) or 242.6 ± 1.3 kcal/mol.⁷ A mean value of Δ*H*_{*f*0}^o(HCS⁺) = 243.2 ± 1.9 kcal/mol would currently be the best estimate. Within the uncertainty, this value is essentially that obtained by Butler and Baer⁴ from thiirane, but rejected. In hindsight, their thresholds for HCS⁺ from thietane and tetrahydrothiophene (see especially their Fig. 1) appear to have been chosen far into the thermal tail. With Δ*H*_{*f*0}^o(HCS⁺) = 243.2 ± 1.9 kcal/mol, the predicted I.P.(HCS) becomes > 7.38 ± 0.1 eV.

The adiabatic I.P. of CH₂S is the difference between Δ*H*_{*f*0}^o(CH₂S⁺) and Δ*H*_{*f*0}^o(CH₂S). The latter may be estimated from the proton affinity of CH₂S (Ref. 10) (185.5 ± 1 kcal/mol, corrected to the modern scale) and Δ*H*_{*f*0}^o(CH₂SH⁺) = 211.5 ± 2.0 kcal/mol.¹ Thus Δ*H*_{*f*0}^o(CH₂S) = 30.4 ± 2.2 kcal/mol. The value of Δ*H*_{*f*0}^o(CH₂S⁺) obtained in an earlier study from our laboratory¹¹ is < 241.8 kcal/mol. From these quantities, one would deduce I.P.(CH₂S) < 9.17 ± 0.1 eV, about 0.2 eV lower than the photoelectron spectroscopic values.^{2,3} However, the appearance potential of CH₂S⁺(CH₃SH) on which Δ*H*_{*f*0}^o(CH₂S⁺) is based is highly uncertain. The related fragment yield curve has very pronounced curvature,¹¹ and, with no objective way to establish a rigorous threshold, a value close to the background level had been selected.¹² In order to provide an independent means of establishing Δ*H*_{*f*0}^o(CH₂S⁺), as well as other quantities that enter into these studies, we have examined the photodissociative ionization of methyl disulfide (CH₃SSCH₃) previously reported by Butler *et al.*¹³

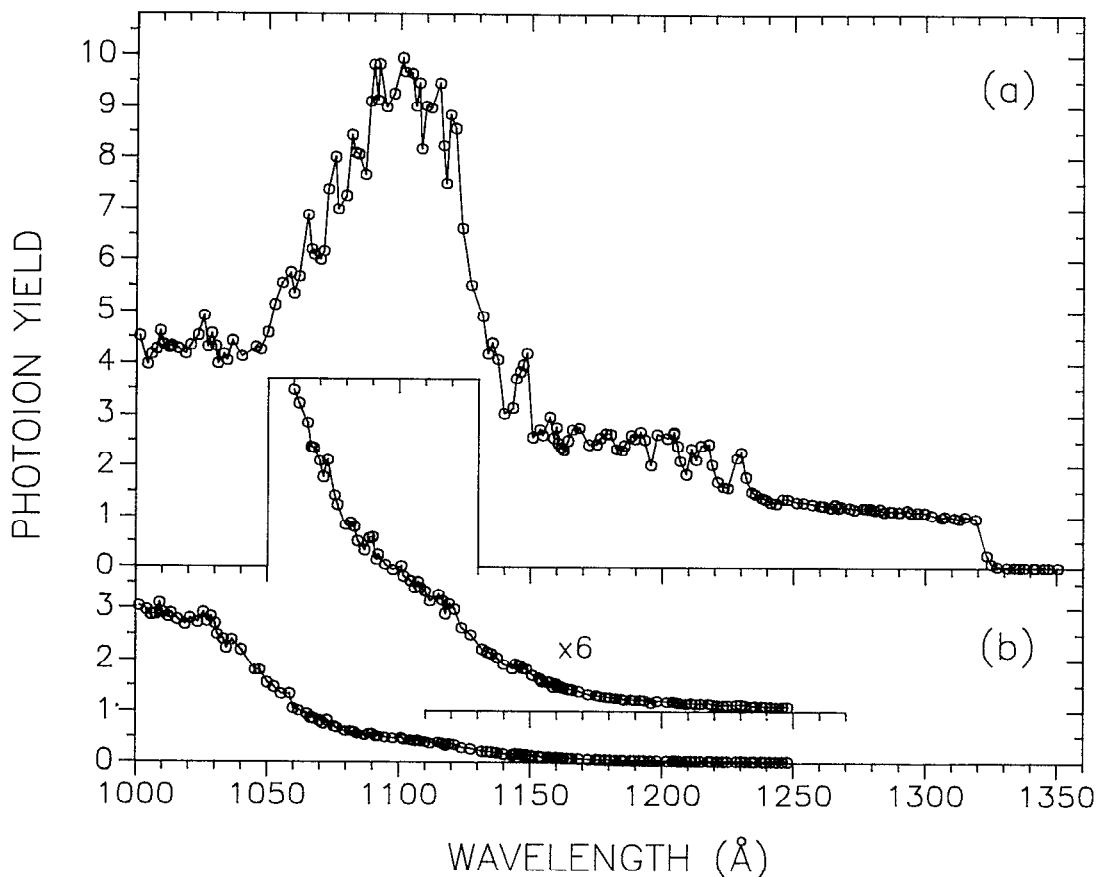


FIG. 1. Photoionization yield curves of CH₂S obtained by pyrolysis of CH₃SSCl at 370 °C. (a) Parent CH₂S⁺. (b) HCS⁺ fragment. The magnified inset in (b) shows two linear regions (1060–1085 Å and 1085–1120 Å) and a long exponential tail which are discussed in the text.

II. EXPERIMENTAL ARRANGEMENT

Both CH₂S and HCS were prepared *in situ* by the reaction of F atoms with methyl mercaptan, CH₃SH. Fluorine atoms were generated by microwave discharge through pure F₂. The description of the discharge tube and reaction cup has been given previously, together with the photoionization mass spectrometer.¹⁴

In a different set of experiments, CH₂S was prepared by pyrolysis of methyl disulfide, CH₃SSCH₃ (at ~650 °C) and methanesulfonyl chloride, CH₃SOCl (at ~540 °C and also at ~370 °C). The pyrolysis oven consisted of a straight quartz tube (~6 mm o.d.) located immediately above an "open" ionization chamber. The bottom section (~10 cm) of the tube was tightly wrapped by a resistive heater and insulated with tantalum foil, leaving an unheated section of ~6 cm immediately above the ionization chamber. During the experiments, the temperature of the oven was monitored with a chromel-alumel thermocouple. An attempt was also made to prepare HCS by reacting CH₂S (produced by pyrolysis) with F atoms. This approach, however, yielded a somewhat lower usable intensity of photoions and substantially higher stray ion background levels than the CH₃SH+F reaction, and was not further pursued.

All chemicals (except CH₃SOCl) were of commercial origin and highest available purity. Small batches of the

methanesulfonyl chloride sample were freshly prepared before each run by chlorination of CH₃SSCH₃ at -17 °C.¹⁵ In order to have better control over the flow rate, CH₃SOCl was admitted into the instrument from a saturated salt/ice slush bath. The measurements were performed utilizing the peak light intensities in the many-line emission spectrum of a discharge in molecular hydrogen. The nominal wavelength resolution was kept at 0.84 Å (full width at half-maximum) throughout all experiments.

III. EXPERIMENTAL RESULTS

A. CH₂S

1. The parent CH₂S⁺ ion

The CH₂S species was most conveniently prepared by pyrolysis of methanesulfonyl chloride, CH₃SOCl. The photoion yield curve of CH₂S⁺ (CH₂S), obtained at ~370 °C, is presented in Fig. 1(a). After the threshold at 1322.3 Å (*vide infra*), the photoion yield curve displays a featureless plateau until ~1235 Å. At ~1230 Å, peaks due to autoionization start appearing and persist until the end of the recorded spectrum (1000 Å). Underlying these peaks, the mildly growing plateau continues until ~1150–1140 Å. At this point, the photoion yield curve starts rising abruptly, reaches a maximum at ~1110–1100 Å, and then sharply

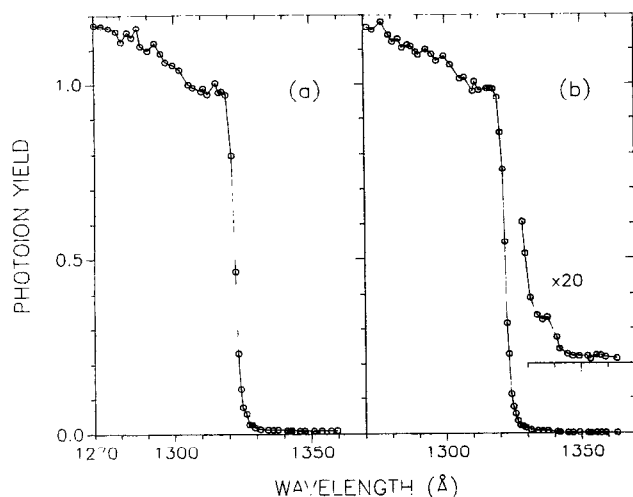


FIG. 2. Photoionization yield curves of CH_2S^+ from CH_2S in the threshold region. (a) Obtained by hydrogen abstraction with F atoms from CH_3SH ; (b) Obtained during pyrolysis of CH_3SSCH_3 at 650°C . The magnified inset shows a weak hot band.

declines until $\sim 1050\text{--}1040\text{ \AA}$, after which it again continues with a mild, gradual growth.

CH_2S was also prepared by reaction of F atoms with CH_3SH , presumably in a two-step hydrogen abstraction. The threshold region, obtained during these experiments, is shown in Fig. 2(a). The photoion yield curve displays an abrupt, steplike onset, characteristic of ionization dominated by the $0\rightarrow 0$ transition. The midrise of the onset in Fig. 2(a) occurs at $1322.3 \pm 0.4\text{ \AA} \equiv 9.376 \pm 0.003\text{ eV}$, and represents the adiabatic I.P. of CH_2S .

An almost identical spectrum of the threshold region, obtained during an experiment where CH_2S was prepared by pyrolysis of methyldisulfide, CH_3SSCH_3 at $\sim 650^\circ\text{C}$, is shown in Fig. 2(b). Here due to the higher temperature of the experiment, a weak hot band [$1341.1 \pm 0.7\text{ \AA}$, shown enlarged in the inset of Fig. 2(b)] is detectable below the threshold. Its intensity is roughly 190 times less than that of the $0\rightarrow 0$ step, and its position corresponds to a frequency of $\sim 1060 \pm 60\text{ cm}^{-1}$ in the neutral.

In both Fig. 2(a) and 2(b), there is a hint of a mild step in the plateau region. This step is centered at $\sim 1304.4 \pm 0.9\text{ \AA}$ and it corresponds to a weak $0\rightarrow 1$ transition with an ion frequency of $1050 \pm 80\text{ cm}^{-1}$ and a Franck–Condon factor ~ 11 times lower than that of the $0\rightarrow 0$ transition.

If we assume that the Franck–Condon factors for the $0\rightarrow 1$ and $1\rightarrow 0$ transitions are essentially the same, then the ratio of the intensities of the $0\rightarrow 1$ step and the hot band suggests a Boltzmann temperature of $\sim 270^\circ\text{C}$. This is significantly lower than the oven temperature ($\sim 650^\circ\text{C}$), and can be attributed to collisional cooling in the final unheated portion of the quartz oven (see Sec. II).

2. The HCS^+ fragment from CH_2S

An initial attempt to determine accurately the appearance potential of the HCS^+ fragment from CH_2S was carried out during the experiments involving the pyrolysis of

CH_3SSCH_3 . However, the HCS^+ ion yield curve displayed a very long, albeit weak, tail extending to much lower energies than expected. Ion–molecule reactions, suspected initially as possible culprits, were ruled out after it was established that the $\text{HCS}^+/\text{CH}_2\text{S}^+$ ratio in the tail did not change appreciably over a pressure range varying by roughly a factor of 30. Variations of repeller settings and pyrolysis temperatures also had no significant influence on the tail region. Although the main products of the pyrolysis of CH_3SSCH_3 were CH_2S and CH_3SH , more than a dozen other parents and/or fragments could be detected at $\sim 11\text{ eV}$ ionization energy, suggesting that the tail originated from some other species emanating from the oven.

Next, a pyrolysis of CH_3SCl was attempted. This system provided a substantially “cleaner” source of CH_2S : In addition to CH_2S and its counterpart, HCl , the main impurity detected was CS_2 . Nevertheless, the HCS^+ fragment curve was very similar to that obtained during the CH_3SSCH_3 pyrolysis. Again, different pressures and oven temperatures were explored, but the origin of the long tail could not be determined. Finally, the spectrum was recorded at two temperatures (~ 540 and $\sim 370^\circ\text{C}$) and found to differ only slightly.

The possibility that at least a portion of the tail intensity originates in an ion-pair process ($\text{CH}_2\text{S} + h\nu \rightarrow \text{HCS}^+ + \text{H}^-$) was also tested. However, at a few intense light peaks in the region of $1090\text{--}1120\text{ \AA}$, only a barely detectable H^- signal was observed, with an intensity ~ 4 orders of magnitude weaker than the CH_2S^+ parent, and at least a factor of 400 lower than the intensity of the HCS^+ tail.

The overall curve of the HCS^+ fragment, obtained at $\sim 370^\circ\text{C}$, is shown in Fig. 1(b). The contribution of HCS^+ from unpyrolyzed CH_3SCl is relatively insignificant and amounts to $\sim 6\%$ of the total HCS^+ signal at 1015 \AA , $\sim 14\%$ in the region $1080\text{--}1085\text{ \AA}$, $\sim 9\%$ at 1100 \AA , and $\sim 13\%$ at 1130 \AA .

At the shortest explored wavelength, the intensity of the HCS^+ fragment is $\sim 65\%\text{--}70\%$ of the parent CH_2S^+ . Going toward longer wavelength, the ion yield curve remains relatively flat until $\sim 1030\text{ \AA}$, and then dips toward $\sim 1085\text{ \AA}$. The last section of this decline, $\sim 1060\text{--}1085\text{ \AA}$, seems almost linear. At $\sim 1085\text{ \AA}$ a change in slope occurs [see expanded inset of Fig. 1(b)], and another quasilinear portion ensues until $\sim 1120\text{ \AA}$. Beyond $\sim 1120\text{ \AA}$, the ion yield curve decays exponentially and maintains at longer wavelengths a very weak, but measurable intensity, even when the incomplete separation of $m/e=45$ (HCS^+) and 46 (CH_2S^+) in our quadrupole mass filter is taken into account.

The shape of the fragment curve suggests that the growth of the ion yield beginning at $\sim 1085\text{ \AA}$ and continuing to shorter wavelength represents the fragment HCS^+ from CH_2S , while the section between ~ 1085 and $\sim 1120\text{ \AA}$ together with the exponential tail to longer wavelengths represents a spurious “background” of unknown origin. Thus we choose as a significant threshold the point of intersection of the linear ascent between $\sim 1060\text{--}1085\text{ \AA}$ and a linear sloping background extending to $\sim 1120\text{ \AA}$ (see Fig. 3). By least squares fitting, this

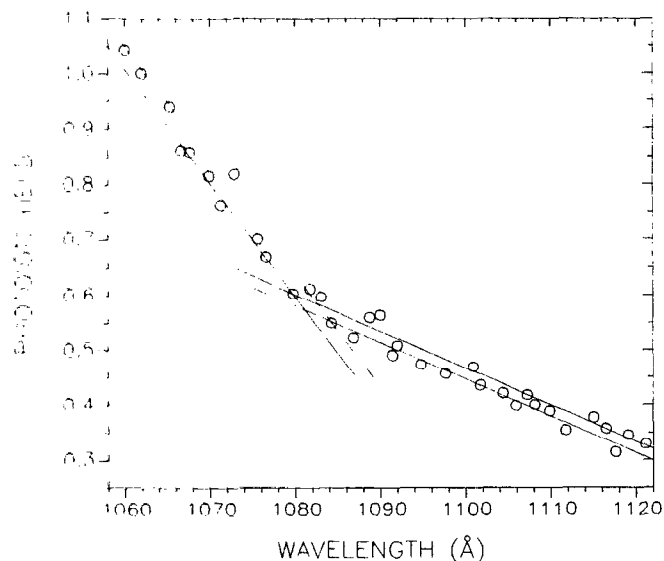


FIG. 3. Expanded view of the relevant portion of the curve from Fig. 2(b) (HCS⁺ fragment from CH₂S). The lines are least squares fits to a presumed background and a quasilinear fragmentation onset. The intersection corresponds to the fragment threshold.

intersection is found to occur at $1081.9 \pm 1.5 \text{ \AA} \equiv 11.460 \pm 0.016 \text{ eV}$.

Based on the shape of the fragment curve, the only other possible choice for this threshold would be somewhere deep in the exponential tail region, at $\lambda > 1180 \text{ \AA}$, giving an A.P. $< 10.5 \text{ eV}$. This, however, would be implausibly low (by $> 15\text{--}20 \text{ kcal/mol}$), when compared to the current best estimates of $\Delta H_f^\circ(\text{CH}_2\text{S})$ and $\Delta H_f^\circ(\text{HCS}^+)$ given in Sec. I.

In Sec. III A 1 we have shown that the Boltzmann temperature of the CH₂S molecules in the ionization chamber was considerably lower than the nominal oven temperature, due to collisional cooling in the unheated section of the quartz tube. Assuming a simple dependence between the degree of cooling and the difference in temperature of the heated and unheated section, one can infer that the Boltzmann temperature of the CH₂S sample during the present experiment was about 150–190 °C. With known frequencies of CH₂S,¹⁶ this results in an internal energy correction of $0.074 \pm 0.005 \text{ eV}$. Therefore, the appearance potential of HCS⁺ from CH₂S, at 0 K, is $\leq 11.533 \pm 0.021 \text{ eV}$.

B. HCS⁺ from HCS

During some of the CH₃SH + F experiments, a measurable ion signal at $m/e=45$, attributable to HCS⁺ from HCS, could be detected at wavelengths above $\sim 1400 \text{ \AA}$. The prerequisites were a particularly favorable surface condition in the reaction cup and a relatively intense production of F atoms. With these conditions, the hydrogen abstraction of CH₃SH (presumably involving surface reactions) could be nominally carried over three steps, generating the HCS radical. Even under the best of circumstances, the relative abundance of the HCS species was extremely weak.

The resulting photoion yield curve (Fig. 4) displays a general decline toward lower energy. Although somewhat masked by the presence of autoionization peaks, an underlying steplike structure can be discerned. Ignoring the apparent threshold at $\sim 1650 \text{ \AA}$, the first step occurs between 1630 and 1640 Å, with a midrise point at $1634.3 \pm 0.7 \text{ \AA} \equiv 7.586 \pm 0.003 \text{ eV}$. The next step, at 1615.5 ± 1.5

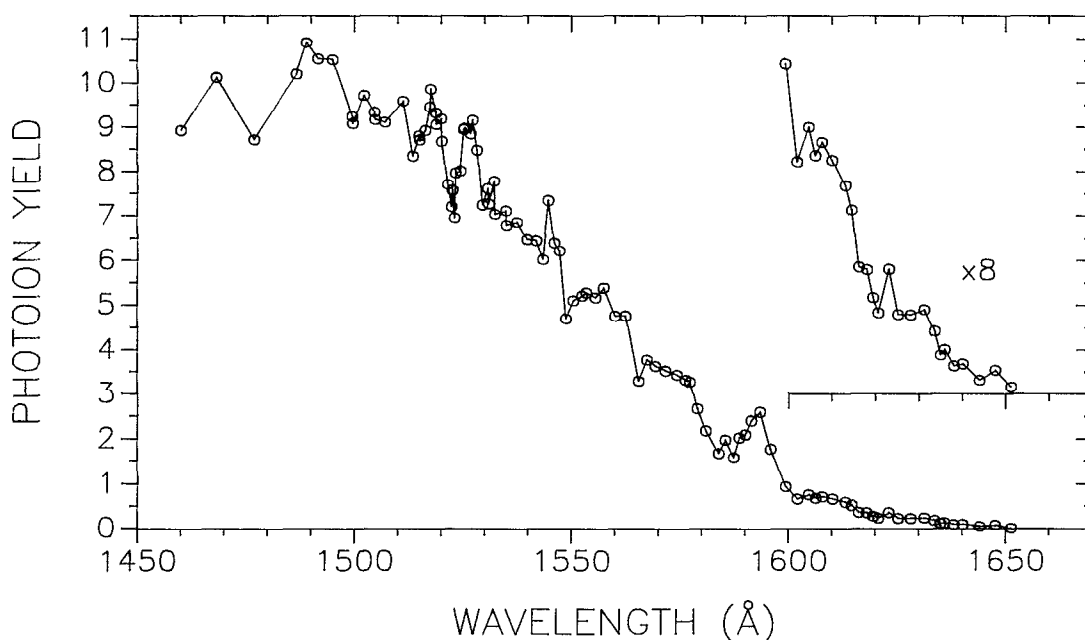


FIG. 4. Photoionization yield curve of HCS⁺ from HCS, obtained during hydrogen abstraction reactions from CH₃SH.

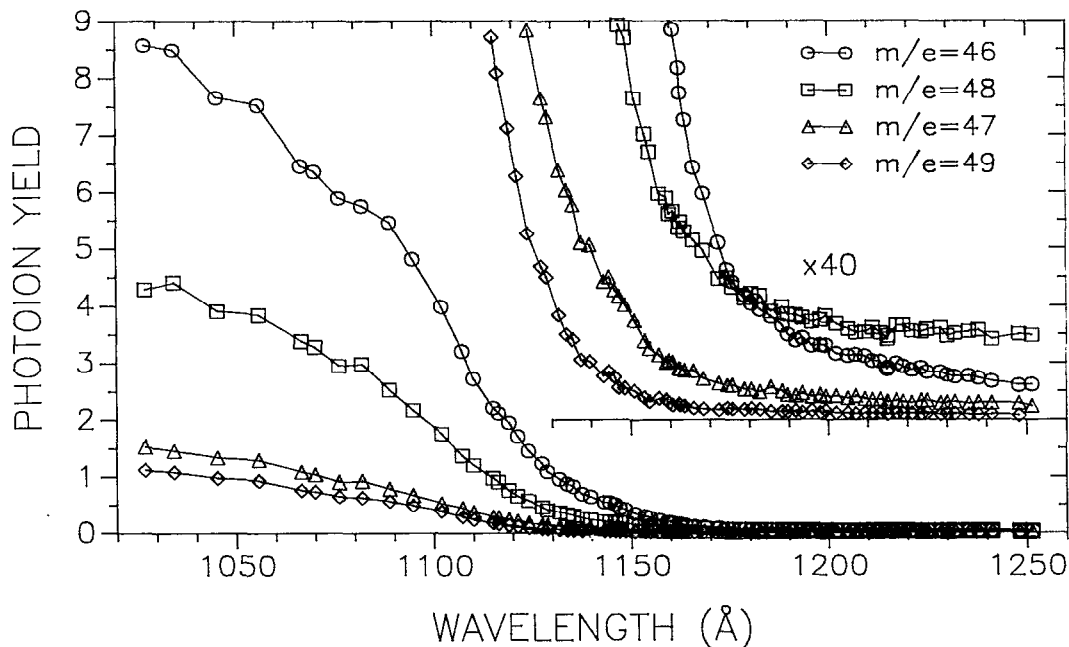


FIG. 5. Fragment yield curves from CH₃SSCH₃ (circle: $m/e=46$, square: $m/e=47$, triangle: $m/e=48$, diamond: $m/e=49$).

$\text{\AA} \equiv 7.675 \pm 0.007$ eV, is quite rounded, and is followed by a step at 1598.4 ± 0.7 $\text{\AA} \equiv 7.757 \pm 0.003$ eV, which then merges into an autoionizing resonance. Two more steps are visible at 1580.0 ± 0.7 $\text{\AA} \equiv 7.847 \pm 0.003$ eV and at 1563.4 ± 0.7 $\text{\AA} \equiv 7.930 \pm 0.003$ eV. The next step, at ~ 1545 \AA is almost completely masked by a resonance peak, and any further steps are difficult to discern. The average distance between the steps is 0.087 ± 0.004 eV = 700 ± 30 cm⁻¹.

The underlying staircase structure, corresponding to direct ionization, is a manifestation of a very broad Franck-Condon distribution and reflects a significant change in geometry. The apparent threshold at ~ 1650 \AA , is very weak and cannot be *a priori* interpreted as the adiabatic ionization onset. The problem arises because of declining Franck-Condon factors, low abundance of the HCS species and low light intensity in this region. Presumably, the true adiabatic threshold could be occurring at even lower energies, with a vanishingly small Franck-Condon factor. Alternatively, the tail above ~ 1640 \AA might be attributed to a hot band contribution. Thus from the observed steplike features alone, we can conclude only that $\text{I.P.}(\text{HCS}) \leq 7.586 \pm 0.003$ eV, and is perhaps lower by one or more vibrational quanta of magnitude 0.087 ± 0.004 eV.

In the past, we have found that the species emanating from our reaction cup have a Boltzmann temperature very near to 300 K (presumably due to multiple collisions with the walls of the reaction cup). If the residual tail in the 1640–1650 \AA region were to correspond to a hot band, then the 0→0 transition would occur at 1634.3 \AA and the 0→1 transition at 1615.5 \AA . The step height (proportional to the Franck-Condon factor) of the presumed 0→1 transition is (in arbitrary units of Fig. 4) 0.44–0.48. Assuming that the Franck-Condon factor for a 1→0 transition is

similar to that of a 0→1 transition, leads to an estimated intensity for a hot band of ~ 0.015 , or at most 0.02 (in the same arbitrary units). The measured intensity in the “tail” is 0.04–0.08, i.e., ~ 2 –5 times more intense, and would correspond to a Boltzmann temperature of ~ 500 K. This makes the hot band hypothesis unlikely.

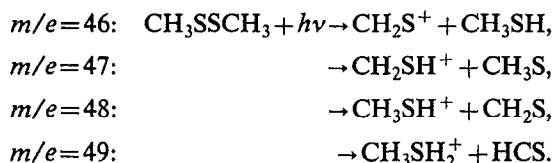
The inference deduced above can be refined by a Franck-Condon analysis. In most cases the Franck-Condon factors are approximated fairly well by a Poisson distribution, $a^n/n!$. If the adiabatic threshold is picked as 1634.3 ± 0.7 \AA , the resulting Franck-Condon distribution cannot be fitted even in the crudest manner by a Poisson series, regardless of the choice of the parameter a . Thus the adiabatic ionization potential of HCS has to be at least one vibrational quantum lower, i.e., $\text{I.P.}(\text{HCS}) \leq 7.499 \pm 0.005$ eV. With this selection for the threshold, the experimental Franck-Condon factors can be fitted reasonably well (within the expectations of such a simple model) by a Poisson distribution with $a=5.6$ –5.8. When the adiabatic I.P. is lowered by yet another vibrational quantum, to 7.412 ± 0.007 eV, the Poisson distribution once again fits the Franck-Condon factors fairly well (only now with $a=7.4$ –7.8). While 7.499 eV corresponds to a threshold in the neighborhood of our last experimental point, an I.P. of 7.412 would imply that the plateau between 1640 and 1650 \AA is followed by another one, which is almost 1 order of magnitude weaker. Recalling the experimental limitations mentioned before, it would be extremely difficult for us to ascertain the existence of this additional step.

If the threshold is shifted to still lower energies, one encounters again a very poor fit to the resulting Poisson distribution. Therefore, it can be safely concluded that $\text{I.P.}(\text{HCS}) \leq 7.499 \pm 0.005$ eV, and possibly 7.412 ± 0.007 eV. Although the latter gives a slightly better Poisson fit, a

clear choice between the two possibilities cannot be made with this simplified harmonic model analysis.

C. Photodissociative ionization of CH₃SSCH₃

We focus our attention here on four fragments ($m/e=46-49$), whose appearance potentials are close to one another. The dissociative ionization processes associated with these masses are as follows:

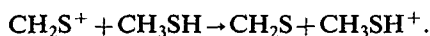


The corresponding photoion yield fragment curves are shown in Fig. 5. All have substantial curvature as they approach the background level. In addition, the $m/e=48$ curve displays a small constant background offset (noticeable in the magnified inset of Fig. 5), which is unrelated to the $\text{CH}_3\text{SSCH}_3 \rightarrow \text{CH}_3\text{SH}^+ + \text{CH}_2\text{S}$ process and probably arises from an impurity in the sample. To a much smaller degree, the same is true for the $m/e=47$ curve.

Butler *et al.*¹³ have previously examined these processes, and obtained appearance potentials by linear extrapolation. Given the pronounced curvature, this approach seems uncertain, since one has a choice of "linear" segments, which depends upon the sensitivity of the apparatus and the degree of expansion of the ordinate. Also, one can expect that these fragments will be subject to considerable retardation (i.e., kinetic shifts).

Here we attempt a different approach, which bears some resemblance to the method of extrapolated differences utilized in earlier electron impact studies. We try to match the curvatures of the respective photoion yield curves for masses 46–49, and thereby determine the relative shift between the respective appearance potentials. These shifts correspond to enthalpies of hypothetical reactions equating the products of two different fragmentation channels.¹⁷

For example, the shift on the energy scale necessary to superimpose the curves for $m/e=46$ and $m/e=48$, $\Delta H_r(46,48)$, corresponds to the enthalpy (at 0 K) of the following reaction:



This particular example is a charge transfer reaction, and its enthalpy can be readily calculated from the difference in ionization potentials of CH₃SH [9.440 ± 0.002 eV (Ref. 11)] and CH₂S (9.376 ± 0.003 eV, see Sec. III A 1) to be 1.48 ± 0.08 kcal/mol.

To implement the curve-matching technique, we normalize the four fragment curves in such a way that they attain the same intensity at ~1030 Å (which is a relatively short wavelength). This involves amplifying the relative intensities of $m/e=47, 48$, and 49 by 5.75, 1.96, and 7.83, respectively. In addition, $m/e=47$ and 48 have to be slightly shifted downwards, in order to compensate for the

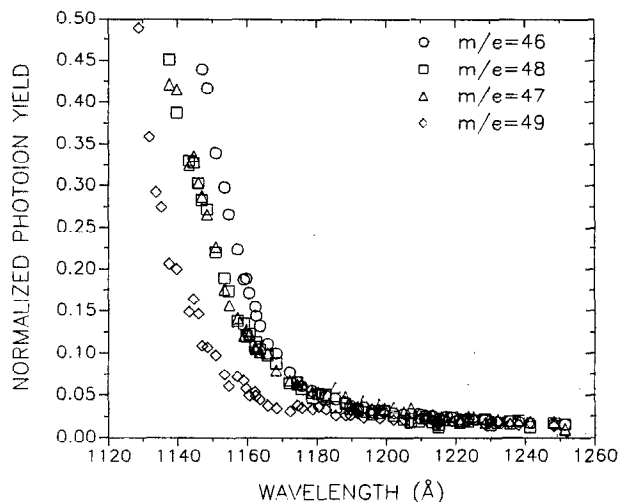


FIG. 6. Normalized fragment yield curves from CH₃SSCH₃. The symbols are the same as in Fig. 5. The normalization procedure, described in the text, is performed in such a way that all four curves match in intensity at ~1030 and ~1250 Å.

spurious background offsets present in the data. The result of this normalization procedure is shown in Fig. 6. Now we can try to match the curvatures of a chosen pair of masses near threshold, by sliding one curve along the wavelength axis until it fits most closely the other curve. The latter procedure is repeated with several different expansion factors. In the case of $m/e=46$ and 48, the best match is obtained when $m/e=48$ is shifted to longer wavelength by 6 ± 3 Å (see Fig. 7). This translates into $\Delta H_r(46,48) = 1.3 \pm 0.6$ kcal/mol, in very good agreement with the value determined from the known ionization potentials, and given above.

The matching procedure can be continued by inter-comparing all possible pairs of curves. Averaging the var-

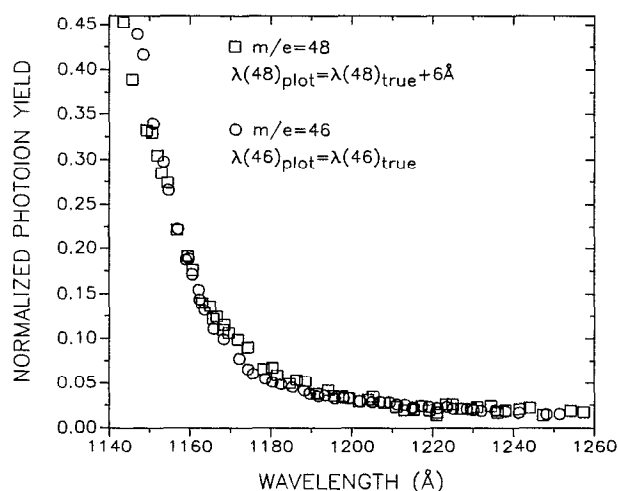
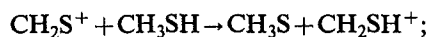
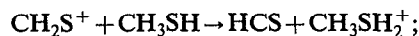


FIG. 7. Determination of the relative shift between normalized fragment curves for $m/e=46$ and 48 from CH₃SSCH₃. In order to achieve a match, the $m/e=48$ fragment curve has been shifted by 6 Å to higher wavelength.

ious shifts, and interconverting them where necessary by using $\Delta H_r(46,48) = 1.5$ kcal/mol, one can obtain the following "consolidated" values:

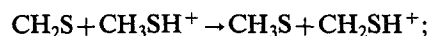


$$\Delta H_r(46,47) = 1.5 \pm 0.7 \text{ kcal/mol},$$

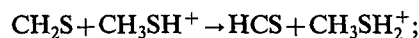


$$\Delta H_r(46,49) = 4.0 \pm 0.8 \text{ kcal/mol}$$

or, equivalently,



$$\Delta H_r(48,47) = 0.0 \pm 0.7 \text{ kcal/mol},$$



$$\Delta H_r(48,49) = 2.5 \pm 0.8 \text{ kcal/mol}.$$

Of these values, the two involving $m/e=49$ have to be regarded with caution, since the curvature associated with this fragment is somewhat different than those of the remaining three fragments. All four curves display an exponential decay pattern near threshold, but $m/e=49$ seems to grow more rapidly than the other three fragments in the initial ascending portion of these curves. This in turn might mean that $m/e=49$ is subject to a smaller kinetic shift than the other fragments, and hence $\Delta H_r(46,49)$ and $\Delta H_r(48,49)$ determined here might be lower than the true thermodynamic differences.

IV. INTERPRETATION OF RESULTS

A. CH₂S

In Sec. III A 1 we have shown that the adiabatic I.P. of CH₂S is 9.376 ± 0.003 eV, and that the threshold region is dominated by the 0→0 transition. The latter feature is in complete agreement with the photoelectron spectra,^{2,3} which display a very prominent 0→0 peak. Also, our I.P. is in essential agreement with the PES value of Solouki *et al.*³ (9.38 eV, with no error bar given). Both values are listed in Table I. The older PES value of 9.34 ± 0.01 eV by Kroto and Suffolk² (also listed in Table I) is slightly lower, presumably due to a concomitant CH₃SH impurity partly masking the region of interest.

As outlined before, our photoionization spectrum shows a 0→1 step which is ~11 times weaker than the 0→0 step (see Fig. 2). The newer PES spectrum by Solouki *et al.*³ also displays a 0→1 peak which is about 1 order of magnitude weaker than the 0→0 peak. These authors found a spacing of 935 ± 100 cm⁻¹ between the peaks, somewhat lower than our value of 1050 ± 80 cm⁻¹, but still in rough agreement when both error bars are considered. Our ionic value is essentially the same as the value for the neutral, inferred from the hot band (1060 ± 60 cm⁻¹).

Since in photoionization the 0→0 transition is dominant, one expects a very small change in structure between the ground state of the neutral and the ion. The active frequency is easily identified as the C–S stretch, known to

TABLE I. Experimental values of ionization potentials (in eV) for the CH_nS and CH_nO species.

CH ₃ SH	9.440 ± 0.002^a 9.446 ± 0.010^b	CH ₃ OH	10.85 ± 0.01^c
CH ₃ S	9.262 ± 0.005^d 9.225 ± 0.014^e	CH ₃ O	10.726 ± 0.008^f
CH ₂ SH	7.536 ± 0.003^d	CH ₂ OH	$7.549 \pm 0.006^{f,g}$ 7.56 ± 0.01^h
CH ₂ S	9.376 ± 0.003^i 9.38^j 9.34 ± 0.01^k	CH ₂ O	10.874 ± 0.002^c
HCS	$<7.499 \pm 0.005^i$ $(7.412 \pm 0.007)^i$	HCO	8.14 ± 0.04^l

^aReference 11.

^bFrom S. Nourbakhsh, K. Norwood, H.-M. Yin, C.-L. Liao, and C. Y. Ng, *J. Chem. Phys.* **95**, 946 (1991).

^cReference 26.

^dReference 1.

^eFrom S. Nourbakhsh, K. Norwood, G.-Z. He, and C. Y. Ng, *J. Am. Chem. Soc.* **113**, 6311 (1991).

^fReference 38 gives I.P.(CD₃O) = 10.726 ± 0.008 eV and I.P.(CD₂OH) = 7.540 ± 0.006 eV, as well as isotopic shifts expected from ZPE differences.

^gB. Ruscic and J. Berkowitz, *Prepr. Div. Fuel Chem. Am. Chem. Soc.* **36**, 1571 (1991) report I.P.(CH₂OH) listed here.

^hFrom J. M. Dyke, A. R. Ellis, N. Jonathan, N. Keddar, and A. Morris, *Chem. Phys. Lett.* **111**, 207 (1984).

ⁱThis work.

^jReference 2.

^kReference 3.

^lReference 24.

be 1059.2 cm⁻¹ in the neutral.¹⁶ The ratio of the intensities of the 0→0 and 0→1 transitions implies that the Franck-Condon factors can be represented by a Poisson series with parameter $a \approx 0.09$. Using the simplest harmonic model expression¹⁸ for this parameter, $a = \Delta^2 \mu \nu 2\pi^2 c / h$ (where μ and Δ are the reduced mass and geometry change along the relevant normal coordinate, while ν is the active frequency), one obtains $\Delta \approx 0.025$ Å as the approximate change in the C–S bond length upon ionization.

These inferences are fully supported by *ab initio* calculations,¹⁹ which find that the adiabatic I.P. is 9.38 eV, and that the geometric structures of CH₂S and CH₂S⁺ (in their respective ground states) are almost identical. According to the calculations, the main change upon ionization involves the shortening of the C–S bond by 0.036 Å, in very good agreement with the value derived above.

The overall shape of the photoionization yield curve of CH₂S [see Fig. 1(a)] is very reminiscent of that of CH₂O, measured previously in this laboratory.²⁰ CH₂O also displays an abrupt onset, and a long, slowly ascending plateau with a prominent broad maximum ~2 eV above threshold. The autoionizing features have been identified as vibrational members belonging to the [\tilde{A}^2B_1]3p(a_1), [\tilde{A}^2B_1]ns(a_1), and [\tilde{B}^2B_2]np(b_2) Rydberg states. The states are characterized by quantum defects $\delta_s \sim 1.1$ and $\delta_p \sim 0.8$. This is in very good agreement with the atomic quantum defects for oxygen:²¹ $\delta_s = 1.142$ and $\delta_p = 0.710$.

Although the features in the CH₂S spectrum are not very precisely defined (because measurements have been confined to peak light intensities only), the autoionizing

structure seems to form, at least partly, a similar pattern as in CH₂O. The lowest energy peak occurs at $\sim 1229 \pm 1 \text{ \AA} \equiv 10.088 \pm 0.008 \text{ eV}$. The three peaks that follow (at $\sim 1216 \text{ \AA}$, $\sim 1204 \text{ \AA}$, and $\sim 1192 \text{ \AA}$) are broader and have a complex structure with some signs of splitting. Each of these three peaks appears to be a superposition of at least two Rydberg members.

The peak at $\sim 1229 \text{ \AA}$, together with the maxima of the three peaks that follow, defines a rather regular pattern with a spacing of $\sim 840 \pm 50 \text{ cm}^{-1}$. This spacing is similar to that seen in the second band of the PES spectrum³ ($840 \pm 100 \text{ cm}^{-1}$). One can thus conclude that these peaks represent vibrational components of one or more Rydberg series converging to $\tilde{A}^2 B_1$. When the peak at $\sim 1229 \text{ \AA}$ is tested against this limit (inferred from PES³ to be 11.66 eV), it yields $n^* = 2.94$. The expected atomic quantum defects for sulfur²¹ are $\delta_s = 1.950$, $\delta_p = 1.516$, and $\delta_d = 0.105$. Obviously, the first observed peak is best assigned as the $[\tilde{A}^2 B_1]3d, \nu = 0$ Rydberg state, with a quantum defect of ~ 0.06 . Similarly, the next peak at $\sim 1216 \text{ \AA}$ is a superposition of $[\tilde{A}^2 B_1]3d, \nu = 1$ and $[\tilde{A}^2 B_1]5s, \nu = 0$. The latter Rydberg member has a defect $\delta \sim 1.95$, as expected for an *ns* series. The following two peaks at ~ 1204 and $\sim 1192 \text{ \AA}$ correspond to overlapping $3d, \nu = 2/5s, \nu = 3$, and $3d, \nu = 3/5s, \nu = 4$ members, respectively.

The pattern of peaks changes at $\sim 1179 \pm 2 \text{ \AA}$, where a rather broad peak appears. This peak most probably corresponds to $\nu = 0$ of the first member of a different Rydberg series, with $\nu = 1$ following at $\sim 1167 \pm 2 \text{ \AA}$ and perhaps $\nu = 2$ at $\sim 1156 \pm 3 \text{ \AA}$. The spacing between the peaks is $\sim 860 \pm 70 \text{ cm}^{-1}$. The Rydberg state is characterized by $\delta \sim 1.55$, close to the expected atomic quantum defect for a *p* Rydberg electron, and thus best assigned as $[\tilde{A}^2 B_1]5p, \nu = 0, 1, 2$.

Using 11.66 eV as the limit, a simple extrapolation places $[\tilde{A}^2 B_1]4d, \nu = 0$ and $[\tilde{A}^2 B_1]6s, \nu = 0$ at $\sim 1150 \text{ \AA}$. Indeed, the spectrum shows a prominent peak at $\sim 1148 \pm 2 \text{ \AA}$ with an unresolved shoulder located at $\sim 1145 \pm 2 \text{ \AA}$. Another peak, perhaps corresponding to $\nu = 1$, appears at $\sim 1135 \pm 3 \text{ \AA}$. After that, the peak positions become muddled and a complicated pattern ensues, extending throughout the region of the broad maximum. The next member of the $[\tilde{A}^2 B_1]np, \nu = 0$ series (corresponding to $n = 6$) would be expected at $\sim 1130 \text{ \AA}$, where one can perhaps discern a mild hump on top of a rising baseline.

Clearly, the peaks appearing at energies greater than $\sim 11.5 \text{ eV}$ must mostly correspond to Rydberg series converging to the second excited state of CH₂S⁺. Unfortunately, partly because the value for the $\nu = 0$ limit for this higher state is not entirely clear from the PES spectrum,³ partly because of the complex pattern arising from overlapping peaks, and partly because of the scarcity of experimental points in the spectrum, no reliable assignments for these Rydberg members can be given.

In short, there seems to be some evidence for the existence of vibrational components of *nd* and/or *ns*, as well as *np* Rydberg states converging to the $\tilde{A}^2 B_1$ ionization limit. Although no dependable assignments can be given for corresponding Rydberg states converging to the \tilde{B} state

of CH₂S⁺, one can expect that the related structure follows a similar pattern.

B. HCS

In Sec. III B we have shown that I.P. (HCS) $\leq 7.586 \pm 0.003 \text{ eV}$, based on the photoionization spectrum alone. When Franck–Condon arguments are introduced, one arrives at I.P. (HCS) $\leq 7.499 \pm 0.005 \text{ eV}$, and perhaps $7.412 \pm 0.007 \text{ eV}$ (see also Table I). The latter value is in fortuitously good agreement with the *ab initio* result¹⁹ of 7.41 eV , although both experimental values fall within the typical error bar ($\pm 0.1 \text{ eV}$) of the calculation.

The breadth of the Franck–Condon distribution (see Fig. 4 and discussion in Sec. III B) attests to the fact that HCS undergoes a substantial change in geometry upon ionization. This view is fully supported by *ab initio* calculations,¹⁹ which find that HCS⁺ is linear in its ground state, while the neutral counterpart is bent (HCS $\angle = 134.1^\circ$). Apart from the dramatic change in the angle, the calculations predict only a slight shortening of both the C–S bond (0.018 \AA) and C–H bond (0.005 \AA). Thus one can safely conclude that the progression of $0.087 \pm 0.004 \text{ eV} \equiv 700 \pm 30 \text{ cm}^{-1}$, which dominates the photoionization curve, corresponds to the bending vibration of HCS⁺. This vibration is doubly degenerate in HCS⁺, and, at first glance, should not appear excited. One of its components, however, becomes allowed when the lower, common symmetry of both the linear HCS⁺ and bent HCS is considered. The *ab initio* calculation¹⁹ predicts the doubly degenerate bending frequency of HCS⁺ to be 786 cm^{-1} (when the usual scaling factor of 0.89 is applied), close to our experimental value.

In Sec. III B we have shown that the observed Franck–Condon distribution in the photoion yield curve of HCS can be fitted fairly well by a Poisson distribution either with $a = 5.6\text{--}5.8$ when the I.P. is assumed to be $7.499 \pm 0.005 \text{ eV}$, or with $a = 7.4\text{--}7.8$ when the I.P. is lowered to $7.412 \pm 0.007 \text{ eV}$. This analysis can be expanded by computing the related change in angle implied by the fit. The proper procedure would have to make use of a Duschinsky transformation²² which relates the normal modes of the bent neutral HCS to the linear HCS⁺. However, as the parameters of the distribution were derived by using the simplest harmonic model possible, we are justified at this point in ignoring this complication. Thus we will use the expressions pertinent to the bending coordinate of a linear triatomic molecule XYZ. In this approach, the reduced mass μ can be calculated from²³

$$1/\mu = [r_{\text{HC}}^2/m_{\text{S}} + r_{\text{CS}}^2/m_{\text{H}} + (r_{\text{HC}} + r_{\text{CS}})^2/m_{\text{C}}] / (r_{\text{HC}} \cdot r_{\text{CS}}),$$

using bond lengths borrowed from the *ab initio* geometry¹⁹ of HCS⁺ ($r_{\text{HC}} = 1.086 \text{ \AA}$, $r_{\text{CS}} = 1.494 \text{ \AA}$). The quantity Δ in the expression $a = \Delta^2 \nu / 2\pi^2 c / h$ relates to the change in angle δ_{\angle} (in radians) as $\delta_{\angle}^2 = \Delta^2 / (r_{\text{HC}} \cdot r_{\text{CS}})$. With $\nu = 700 \pm 30 \text{ cm}^{-1}$, the range of values $a = 7.4\text{--}7.8$ corresponds to $\delta_{\angle} = 50.8 \pm 1.8^\circ$, implying that the angle in the neutral HCS is $129.2^\circ \pm 1.8^\circ$. Similarly, $a = 5.6\text{--}5.8$ gives $\delta_{\angle} = 44.0^\circ \pm 1.4^\circ$ or an equilibrium angle of $136.0^\circ \pm 1.4^\circ$ for

the neutral. The latter is in excellent agreement with the *ab initio* calculation,¹⁹ which predicts 134.1°. Nevertheless, even this extension of the Franck–Condon analysis cannot distinguish between the two choices for the I.P. with any reasonable certainty. What it does indicate, though, is that the I.P. is neither significantly lower nor higher than 7.4–7.5 eV.

The broad Franck–Condon distribution resulting from a bent to linear transition upon ionization of HCS parallels the situation found by Dyke *et al.*²⁴ in their PES study of the homologous species HCO. In fact, there the adiabatic 0→0 transition was also too weak to be observed directly. By performing a Franck–Condon analysis, they assigned the first observed peak at 8.35±0.01 eV as *v'*=2 and inferred an adiabatic value of 8.14±0.04 eV.

The ground state of HCS⁺ is a singlet, and corresponds to ejection of an unpaired electron from the uppermost singly occupied orbital. Ejection of an electron from the next deeper molecular orbital will yield both a triplet and a singlet state of the cation. In our photoionization spectrum of HCS (see Fig. 4), a number of peaks superimposed on the staircase baseline can be readily discerned. These must correspond to autoionizing states converging to one or several excited states of HCS⁺. Their exact location (and intensity at the apex) is rather uncertain, because only peak intensities in the light spectrum have been utilized to obtain the photoionization yield curve. Starting from the threshold, prominent peaks of differing widths and shapes appear at 1593.5±1.5 Å≡7.781±0.007 eV, 1556±4 Å≡7.97±0.02 eV, 1545±2 Å≡8.03±0.01 eV, 1527±2 Å≡8.12±0.01 eV, and 1518±2 Å≡8.17±0.01 eV. Beyond 1515 Å, the peaks merge and start forming a complex pattern. Besides these strong peaks, the spectrum displays a number of less intense features, whose positions cannot be accurately determined. All of the above, coupled with the anticipation of more than one Rydberg series, each with possible vibrational components, precludes any attempt to give plausible assignments for these peaks. However, if we borrow the quantum defects from CH₂S (see Sec. IV A), we can conclude that the lowest possible effective quantum number is *n**=2.0–2.1 (corresponding to a 4*s* Rydberg member). If we associate this *n** with the lowest energy peak (at 1593.5±1.5 Å), we can obtain an upper value for the possible convergence limit of about 11.03±0.16 eV, or about 3.5–3.6 eV above the first I.P. Another way to estimate the position of the limit (which presumably corresponds to the lowest triplet state of HCS⁺), is to take the difference between $\tilde{X}^1\Sigma^+$ and $\tilde{a}^3\Pi$, states in the isoelectronic neutral molecule CS. Huber and Herzberg²⁵ give this value as 3.4202 eV. Combining this quantity with our I.P.(HCS), yields a value of ~10.9 to 10.8 eV as a very crude estimate for the second I.P. of HCS. For comparison, Curtiss and Pople¹⁹ calculate the lowest triplet state of HCS⁺ to be 3.75 eV above the ground state.

Returning to Table I, which lists the adiabatic ionization potentials for HCS, CH₂S, and other CH_{*n*}S species, it is interesting to note that I.P.(CH₃SH), I.P.(CH₃S), and I.P.(CH₂S) have fairly similar values, characteristic of a

sulfur lone pair orbital. A similar statement can be made for the oxygen homologs, also listed in Table I. CH₂SH has, on the other hand, a much lower I.P., characterized by the unpaired electron localized near the carbon atom. As pointed out previously,¹ this is probably the reason for the similarity between I.P.(CH₂SH) and I.P.(CH₂OH). Perhaps not entirely by coincidence, I.P.(HCS) also has a similar value. However, HCO does not quite seem to follow this pattern, meaning either that the analogy is inappropriate here, or that the true adiabatic I.P. of HCO is perhaps even lower than that inferred by Dyke *et al.*²⁴

C. Thermochemistry

The reaction enthalpy $\Delta H_r(48,47)=0.0\pm 0.7$ kcal/mol, provides us with a link between $\Delta H_{f0}^\circ(\text{CH}_2\text{S})$ and $\Delta H_{f0}^\circ(\text{CH}_2\text{SH}^+)$. Taking $\Delta H_{f0}^\circ(\text{CH}_3\text{SH})=-3.0\pm 0.1$ kcal/mol,^{26,27} I.P.(CH₃SH)=9.440±0.002 eV,¹¹ and $\Delta H_{f0}^\circ(\text{CH}_3\text{S})=31.4\pm 0.5$ kcal/mol,²⁸ one obtains

$$\Delta H_{f0}^\circ(\text{CH}_2\text{S}) = \Delta H_{f0}^\circ(\text{CH}_2\text{SH}^+) - 183.2 \pm 0.9 \text{ kcal/mol.}$$

This relationship is tantamount to taking P.A.₂₉₈(CH₂S)=183.4±0.9 kcal/mol (or 182.0±0.9 kcal/mol at 0 K), slightly lower than the experimental value of 185.5±1.4 kcal/mol obtained by Roy and McMahon,¹⁰ but in excellent agreement with the *ab initio* value,¹⁹ calculated to be 182.3 kcal/mol at 0 K.

Roy and McMahon¹⁰ determined P.A.(CH₂S) through a number of ladder experiments by ion cyclotron single resonance mass spectrometry. Their results clearly place P.A.(CH₂S) between that of CH₃OH (no proton transfer from CH₂SH⁺ observed) and CH₃CHO (proton transfer from CH₂SH⁺ exothermic). With CF₃CO₂C₂H₅, which further narrows the bracketed value, they did observe proton transfer, but with “a positive double resonance response indicative of an endothermic reaction.” Thus they concluded that P.A.(CF₃CO₂C₂H₅) < P.A.(CH₂S) < P.A.(CH₃CHO). Placed on the modern P.A. scale,²⁹ this yields P.A.(CH₂S)=185.5±1.4 kcal/mol. However, the conclusion hinges critically on their interpretation of the observed response with CF₃CO₂C₂H₅. If the proton transfer from CH₂SH⁺ to CF₃CO₂C₂H₅ is nevertheless exothermic, then P.A.(CH₃OH) < P.A.(CH₂S) < P.A.(CF₃CO₂C₂H₅), or P.A.(CH₂S)=183.3±1.4 kcal/mol, which would be in excellent agreement both with our inference from $\Delta H_r(48,47)$ and with the theoretical prediction.

Utilizing our link between $\Delta H_{f0}^\circ(\text{CH}_2\text{S})$ and $\Delta H_{f0}^\circ(\text{CH}_2\text{SH}^+)$ based on $\Delta H_r(48,47)$ and the upper limit for $\Delta H_{f0}^\circ(\text{CH}_2\text{SH}^+) \leq 213.1 \pm 0.2$ kcal/mol [based on A.P.(CH₂SH⁺/CH₃SH) from Kutina *et al.*¹¹], one obtains an upper limit for $\Delta H_{f0}^\circ(\text{CH}_2\text{S}) \leq 29.9 \pm 0.9$ kcal/mol. Similarly, by using our preferred value for $\Delta H_{f0}^\circ(\text{CH}_2\text{SH}^+) = 211.5 \pm 2.0$ kcal/mol,¹ one obtains $\Delta H_{f0}^\circ(\text{CH}_2\text{S}) = 28.3 \pm 2.0$ kcal/mol, in excellent agreement with *ab initio* calculations [29.0 kcal/mol (Ref. 30), 28.7 kcal/mol (Ref. 19)]. Note that the large error bar in our $\Delta H_{f0}^\circ(\text{CH}_2\text{S})$ propagates from the uncertainty associated with $\Delta H_{f0}^\circ(\text{CH}_2\text{SH}^+)$.

TABLE II. Selected experimental enthalpies of formation (at 0 K) of the CH_nS species and their cations (in kcal/mol) and their comparison with theory.

	Experimental ^a	Theoretical ^b
$\Delta H_{f0}^{\circ}(\text{CH}_3\text{SH})$	-3.0 ± 0.1^c	-2.8
$\Delta H_{f0}^{\circ}(\text{CH}_3\text{SH}^+)$	214.7 ± 0.1^d	215.3
$\Delta H_{f0}^{\circ}(\text{CH}_3\text{S})$	31.44 ± 0.54^e	31.6
$\Delta H_{f0}^{\circ}(\text{CH}_3\text{S}^+)$	245.0 ± 0.5^f	244.8
$\Delta H_{f0}^{\circ}(\text{CH}_2\text{SH})$	$<39.3 \pm 0.2^f$	40.6
	37.7 ± 2.0^f	
$\Delta H_{f0}^{\circ}(\text{CH}_2\text{SH}^+)$	$<213.1 \pm 0.2^g$	211.7
	211.5 ± 2.0^f	
$\Delta H_{f0}^{\circ}(\text{CH}_2\text{S})$	$<29.9 \pm 0.9$	29.0 ^h
	28.3 ± 2.0	28.7
$\Delta H_{f0}^{\circ}(\text{CH}_2\text{S}^+)$	$<246.1 \pm 0.9$	245.0
	244.5 ± 2.0	
$\Delta H_{f0}^{\circ}(\text{HCS})$	$<73.3 \pm 1.0$	70.8
	$>69.7 \pm 2.0$	
	71.7 ± 2.0	
$\Delta H_{f0}^{\circ}(\text{HCS}^+)$	243.9 ± 1.2^i	242.6 ± 1.3^j
	$<244.2 \pm 1.0$	241.7
	242.6 ± 2.0	
$\Delta H_{f0}^{\circ}(\text{CS})$	65.8 ± 0.6^k	65.1
$\Delta H_{f0}^{\circ}(\text{CS}^+)$	327.2 ± 0.6^l	328.4

^aThis work, unless otherwise noted.

^bFrom Ref. 19, unless otherwise noted.

^cReferences 26 and 27.

^dUsing I.P.(CH₃SH) = 9.440 ± 0.002 eV from Ref. 11.

^eReference 28.

^fReference 1.

^gBased on A.P.(CH₂SH⁺/CH₃SH) from Ref. 11.

^hReference 30.

ⁱBased on experimental P.A.(CS) = 188.2 kcal/mol from Ref. 6.

^jBased on theoretical P.A.(CS) = 189.5 ± 1.2 from Ref. 7.

^kAverage of values from Refs. 8 and 9.

^lBased on I.P.(CS) = 11.335 eV from Ref. 25.

Using our I.P.(CH₂S) = 9.376 ± 0.003 eV and the above values for $\Delta H_{f0}^{\circ}(\text{CH}_2\text{S})$, one obtains $\Delta H_{f0}^{\circ}(\text{CH}_2\text{S}^+) = 244.5 \pm 2.0$ kcal/mol ($<246.1 \pm 0.9$ kcal/mol), in excellent agreement with the theoretical value¹⁹ of 245.0 kcal/mol. This result calls into question the value $\Delta H_{f0}^{\circ}(\text{CH}_2\text{S}^+) < 241.8 \pm 1.2$ kcal/mol, derived from the threshold of CH₂S⁺ from CH₃SH.¹¹ As outlined in Sec. I, that threshold had been chosen very close to the background level of a photoion yield curve that had very pronounced curvature.¹² Hence, the current value for $\Delta H_{f0}^{\circ}(\text{CH}_2\text{S}^+)$ is to be preferred.

We noted in Sec. I that the value of P.A.(CS) leads to either $\Delta H_{f0}^{\circ}(\text{HCS}^+) = 243.9 \pm 1.2$ kcal/mol [from the experimental P.A.(CS) = 188.2 kcal/mol by Smith and Adams⁶] or $\Delta H_{f0}^{\circ}(\text{HCS}^+) = 242.6 \pm 1.3$ kcal/mol [from the calculated P.A.(CS) = 189.5 ± 1.2 kcal/mol by Botschwina and Sebald⁷]. The latter value is, not surprisingly, closer to the directly calculated *ab initio* value¹⁹ of 241.7 kcal/mol. Using our A.P.(HCS⁺/CH₂S) = 11.533 ± 0.021 eV and $\Delta H_{f0}^{\circ}(\text{CH}_2\text{S}) = 28.3 \pm 2.0$ kcal/mol ($<29.9 \pm 0.9$ kcal/mol) derived above, one obtains $\Delta H_{f0}^{\circ}(\text{HCS}^+) = 242.6 \pm 2.0$ kcal/mol ($<244.2 \pm 1.0$ kcal/mol), in very good agreement with the calculated values (see Table II).

Combining $\Delta H_{f0}^{\circ}(\text{HCS}^+) < 244.2 \pm 1.0$ kcal/mol (= 242.6 ± 2.0 kcal/mol) with I.P.(HCS) = 7.499 ± 0.005

eV (or 7.412 ± 0.007 eV), one obtains $\Delta H_{f0}^{\circ}(\text{HCS}) < 73.3 \pm 1.0$ kcal/mol, $> 69.7 \pm 2.0$ kcal/mol, and 71.7 ± 2.0 kcal/mol as an upper limit, lower limit, and most probable value, respectively. The latter value is in very good agreement with the *ab initio*¹⁹ result, $\Delta H_{f0}^{\circ}(\text{HCS}) = 70.8$ kcal/mol.

Now we would be in a position to check our $\Delta H_r(46,49)$ and $\Delta H_r(48,49)$ values obtained in Sec. III C, if we knew $\Delta H_{f0}^{\circ}(\text{CH}_3\text{SH}_2^+)$. The latter quantity is, however, related to P.A.(CH₃SH). From $\Delta H_r(46,49) = 4.0 \pm 0.8$ kcal/mol (using an estimated 298 to 0 K correction³¹ for P.A. of CH₃SH), one obtains the following relation:

$$\begin{aligned} \text{P.A.}_{298}(\text{CH}_3\text{SH}) &= \Delta H_{f0}^{\circ}(\text{HCS}) - \Delta H_{f0}^{\circ}(\text{CH}_2\text{S}) \\ &+ 146.5 \pm 0.9 \text{ kcal/mol.} \end{aligned}$$

Taking $\Delta H_{f0}^{\circ}(\text{CH}_2\text{S}) = 28.3 \pm 2.0$ kcal/mol and $\Delta H_{f0}^{\circ}(\text{HCS}) = 71.7 \pm 2.0$ kcal/mol, one obtains P.A.(CH₃SH) = 190 ± 3 kcal/mol. Lias *et al.*²⁹ list 187.4 kcal/mol for this quantity. Solka and Harrison³² have found that the free energy change in the proton transfer reactions of CH₃SH₂⁺ with CH₃CHO, C₂H₅CHO, and CH₃OCH₃ are +0.5, -2, and -4 kcal/mol, respectively. Taking (in kcal/mol) P.A.(CH₃CHO) = 186.6, P.A.(C₂H₅CHO) = 189.6, and P.A.(CH₃OCH₃) = 192.1 from Lias *et al.*,²⁹ we obtain P.A.(CH₃SH) = 187.1, 187.6, and 188.1 kcal/mol, respectively, or an average value of 187.6 kcal/mol. No entropy corrections are made here, and hence $\Delta F^0 \approx \Delta H^0$ is assumed. For the proton transfer reaction of CH₃SH₂⁺ with CH₃CHO, Wolf *et al.*³³ obtained $\Delta F^0 = +0.74$ kcal/mol, leading to P.A.(CH₃SH) = 187.3 kcal/mol. Also, they report that ΔH_{300}^0 for the proton transfer reaction between NH₄⁺ and CH₃SH is 16.4 kcal/mol, from which [using P.A.(NH₃) = 204 kcal/mol] one obtains P.A.(CH₃SH) = 187.6 kcal/mol. Hence, P.A.(CH₃SH) = 187.4–187.6 kcal/mol appears to be as accurate as is the proton affinity scale in this region. The calculated¹⁹ P.A.(CH₃SH) is even slightly lower, 185.6 kcal/mol. Thus one can conclude that $\Delta H_r(46,49)$ is in error by ~3–4 kcal/mol. Indeed, by using the theoretical¹⁹ ΔH_{f0}° values for the relevant species, one finds that $\Delta H_r(46,49) = 7$ kcal/mol and $\Delta H_r(48,49) = 5$ kcal/mol, both ~3 kcal/mol higher than the experimental shifts. In Sec. III C we already surmised that this might be possible. The present analysis is essentially suggesting that the CH₃SH₂⁺ fragment from CH₃SSCH₃ is retarded 3–4 kcal/mol less than CH₂S⁺, CH₃SH⁺, and CH₂SH⁺, in spite of the fact that the latter three fragments appear *before* CH₃SH₂⁺. There are different possible reasons for this effect, one of them being that the fragmentation channel leading to CH₃SH₂⁺ proceeds through a “loose” transition complex, while CH₂S⁺, CH₃SH⁺, and CH₂SH⁺ are connected to a similar, “tight,” transition state (or states).

Accepting the selected enthalpies of formation from Table II (and using some auxiliary values^{34–37}), one can calculate various bond energies for the CH_nS system. These are presented in Table III. Previously¹ we have found $D_0(\text{H}-\text{CH}_2\text{SH}) = 92.4 \pm 2.0$ kcal/mol ($< 94.0 \pm 0.1$ kcal/

TABLE III. Selected values for bond dissociation energies at 0 K (in kcal/mol) for the CH_nS system and their comparison with theory.

	Experimental ^a	Theory ^b
$D_0(\text{H}-\text{CH}_2\text{SH})$	<94.0±0.1 ^c 92.4±2.0 ^c	95.0
$D_0(\text{H}-\text{CH}_2\text{S})$	<50.1±1.0 48.5±2.0	48.7
$D_0(\text{H}-\text{HCS})$	<95.0±0.5 ^d >93.0±0.5 ^d 94.0±1.2 ^c	93.7
$D_0(\text{H}-\text{CS})$	<47.7±2.0 >44.1±1.2 45.7±2.0	46.0
$D_0(\text{CH}_3\text{S}-\text{H})$	86.1±0.6 ^f	86.0
$D_0(\text{CH}_2\text{S}-\text{H})$	<43.8±2.0 >40.6±2.0 42.2±2.0	39.7
$D_0(\text{H}_3\text{C}-\text{SH})$	72.6±0.7	73.1
$D_0(\text{H}_2\text{C}-\text{SH})$	>88.1±0.9 89.7±2.0	...
$D_0(\text{H}_3\text{C}-\text{S})$	70.0±0.6	...
$D_0(\text{H}_2\text{C}-\text{S})$	>129.4±1.1 131.0±2.0	131.6
$D_0(\text{HC}-\text{S})$	>134.3±1.0 >137.9±2.0 135.9±2.0	136.0
$D_0(\text{C}-\text{S})$	169.8±0.6	170.5

^aUnless otherwise noted, based on enthalpies of formation listed in Table II, and auxiliary data from Refs. 34–37.

^bReference 19.

^cReference 1.

^dBased on A.P.(HCS⁺/CH₂S) <11.533±0.021 eV and I.P.(HCS) <7.499±0.005 eV (7.412±0.007 eV).

^eAverage of the upper and lower limit.

^fBased on $\Delta H_{70}^\circ(\text{CH}_3\text{S}) = 31.4 \pm 0.5$ kcal/mol from Ref. 28; see also Ref. 1.

mol). Now we can add $D_0(\text{H}-\text{HCS}) = 94.0 \pm 1.2$ kcal/mol. Not surprisingly, the bond strength is similar in both cases. It also compares well with the homologous $D_0(\text{H}-\text{CH}_2\text{OH}) = 95.0 \pm 0.7$ kcal/mol, which can be obtained by subtracting our previously determined³⁸ I.P.(CH₂OH) (see Table I) from A.P.(CH₂OH⁺/CH₃OH) = 11.67 ± 0.03 eV.³⁹ On the other hand, one expects the O–H bond in CH₃OH to be significantly stronger than the S–H bond in CH₃SH. This has been found to be the case, since $D_0(\text{CH}_3\text{S}-\text{H}) = 86.1 \pm 0.6$ kcal/mol,^{1,28} while $D_0(\text{CH}_3\text{O}-\text{H}) = 103.1 \pm 1.0$ kcal/mol, based on $\Delta H_{70}^\circ(\text{CH}_3\text{O}) = 5.9 \pm 1.0$ kcal/mol,³⁸ and $\Delta H_{70}^\circ(\text{CH}_3\text{OH}) = -45.6 \pm 0.1$ kcal/mol.²⁶

The lower half of Table III deals with C–S bond energies. Their values clearly indicate that while in CH₃SH, CH₃S, and CH₂SH, the C–S bond is essentially single (with CH₂SH having perhaps a slightly higher bond order), it has a double bond character in CH₂S and HCS, while CS acquires a triple bond character.

Returning to the upper half of Table III, one notices that the C–H bond energies in CH₃S and HCS are significantly lower than those in CH₃SH and CH₂S. The reason for this behavior is obvious: The C–H bond dissociations are accompanied by a strengthening of the C–S bond in the former two cases, but not in the latter two. A similar rea-

soning applies also to the S–H bond strengths in CH₂SH and CH₃SH. As a consequence, the sequence $D_0(\text{H}-\text{CH}_n\text{S})$, $n=2,1,0$, oscillates between a high and a low value. The same effect is present in many other systems, most notably C₂H_n and Si₂H_n.⁴⁰

V. CONCLUSIONS

The present photoionization measurements yield I.P.(CH₂S) = 9.376 ± 0.003 eV, in excellent agreement with one³ of the previous PES values. The threshold behavior implies a very small change in geometry upon ionization. The overall shape of the photoion yield curve is similar to that of the homologous CH₂O. Evidence has been found for $\bar{n}d$ and/or ns and np Rydberg states converging to the \bar{A} state of CH₂S⁺. These Rydberg states display a broad vibrational envelope, similar to that of the second system in the PES spectrum. In addition, the HCS⁺ fragment from CH₂S has been determined to appear at <11.533 ± 0.021 eV. The adiabatic I.P. of HCS has not been determined directly by photoionization, mainly because of very low Franck–Condon factors at threshold. The very broad vibrational envelope observed in photoionization is consistent with a bent to linear transition. A simple Poisson fit to the experimental Franck–Condon factors implies I.P.(HCS) <7.499 ± 0.005 eV, and perhaps 7.412 ± 0.007 eV. The fragment curves of $m/e=46, 47, 48$, and 49 from CH₃SSCH₃ also have been measured, and their relative shifts determined. Together with I.P.(CH₂S), I.P.(HCS), and A.P.(HCS⁺/CH₂S), this is sufficient to determine the enthalpies of formation of CH₂S and HCS (and their cations), if the previously selected value¹ of $\Delta H_{70}^\circ(\text{CH}_2\text{SH}^+) = 211.5 \pm 2.0$ kcal/mol (<213.1 ± 0.2 kcal/mol) is accepted. When compared to recent *ab initio* calculations,¹⁹ the results show, in general, very good agreement. The present measurements complement our recent work on CH₂SH/CH₃S (Ref. 1) and CH₂OH/CH₃O,³⁸ and extend the list of bond energies within the CH_nS system.

This work was supported by the U. S. Department of Energy, Office of Basic Energy Sciences, under Contract No. W-31-109-ENG-38.

¹B. Ruscic and J. Berkowitz, J. Chem. Phys. **97**, 1818 (1992).

²H. W. Kroto and R. J. Suffolk, Chem. Phys. Lett. **15**, 545 (1972).

³B. Solouki, P. Rosmus, and H. Bock, J. Am. Chem. Soc. **98**, 6054 (1976).

⁴J. J. Butler and T. Baer, J. Am. Chem. Soc. **104**, 5016 (1982).

⁵J. J. Butler and T. Baer, J. Am. Chem. Soc. **102**, 6764 (1980).

⁶D. Smith and N. G. Adams, J. Phys. Chem. **89**, 3964 (1985).

⁷P. Botschwina and P. Sebald, J. Mol. Spectrosc. **110**, 1 (1985).

⁸P. Coppens, J. C. Reynaert, and J. Drowart, J. Chem. Soc. Faraday Trans. II **75**, 292 (1979).

⁹J. H. D. Eland and J. Berkowitz, J. Chem. Phys. **70**, 5151 (1979).

¹⁰M. Roy and T. B. McMahon, Org. Mass Spectrom. **17**, 392 (1982).

¹¹R. E. Kutina, A. K. Edwards, G. L. Goodman, and J. Berkowitz, J. Chem. Phys. **77**, 5508 (1982).

¹²The lower panel of Fig. 3 in Ref. 11 depicts the threshold region of the CH₂S⁺ fragment yield curve from CH₃SH. It can be seen there that a very rounded onset is followed by a brief linear region which ends in a cusp. The linear region relates to the onset of the \bar{A} state in CH₂SH⁺, while the cusp relates to the opening of the next fragmentation channel, leading to CH₂SH⁺. The shape of the tail is governed both by thermal

- effects and the nature of the process. The true threshold for CH₂S⁺ occurs in a Franck-Condon gap between the \tilde{X} and \tilde{A} states of CH₃SH⁺. This makes the initial intensity weak and emphasizes the thermal effects. In addition, the transition state leading to the CH₂S⁺ fragment is very "tight," because it corresponds to a sterically hindered 1,2 elimination of H₂. This also contributes significantly to the roundness of the tail. The reported appearance potential corresponds to a threshold selection deep into the tail, very close to the first departure from the background level. Although the listed value should, perhaps, have been considered as a lower limit, in this case there are still no better or more rigorous ways to select a threshold. Incidentally, Ref. 11 derives $\Delta H_{f0}^{\circ}(\text{CH}_2\text{S}) = 33.1 \pm 1.5$ kcal/mol. Besides the fact that this value was based on too low an appearance potential, which was then combined with an estimated I.P. (CH₂S) = 9.30 eV (also too low), an inadvertent arithmetic error must have occurred. With the same assumptions, the correctly calculated value would be $\Delta H_{f0}^{\circ}(\text{CH}_2\text{S}) = 27.3 \pm 1.5$ kcal/mol. The latter is fortuitously close to $\Delta H_{f0}^{\circ}(\text{CH}_2\text{S})$ which is derived in the present paper, due to cancellation of errors.
- ¹³ J. J. Butler, T. Baer, and S. A. Evans, Jr., *J. Am. Chem. Soc.* **105**, 3451 (1983).
- ¹⁴ S. T. Gibson, J. P. Greene, and J. Berkowitz, *J. Chem. Phys.* **83**, 4319 (1985); J. Berkowitz, J. P. Greene, H. Cho, and B. Ruscic, *ibid.* **86**, 1235 (1987).
- ¹⁵ The synthesis of methanesulfonyl chloride was performed by reacting gaseous chlorine with methyl disulfide. Rather than determining the stoichiometric amount of chlorine (by liquifying and weighing), gaseous chlorine was slowly admitted into a test tube containing methyl disulfide which was immersed in a saturated salt/ice slush bath. When solid methylsulfur trichloride evolved, the chlorine flow was halted, and the test tube shaken to allow the solid to react. More gaseous chlorine was added and the procedure repeated until the solid stopped disappearing. At that point, the clear reddish liquid CH₃SCl was carefully decanted into another test tube and immediately reimmersed into the cold bath. For alternative synthetic routes and the chemistry behind the chlorination, see I. B. Douglass, in *Organic Sulfur Compounds*, edited by N. Kharash, Vol. 1 (Pergamon, Oxford, 1961), p. 350. See also I. B. Douglass, *J. Org. Chem.* **24**, 2004 (1959).
- ¹⁶ D. J. Clouthier and D. A. Ramsay, *Ann. Rev. Phys. Chem.* **34**, 31 (1983).
- ¹⁷ The strategy of equating relative threshold differences with enthalpies of hypothetical reactions assumes that the reverse activation energies of the fragmentation processes which are being compared are zero, or (more rigorously) the same. However, it does not require a knowledge of the heat of formation of the parent, nor that of the products, since only a relative energy is determined. Note also that all the experimental fragment curves are thermally shifted by the (same) amount of available internal energy of the parent. As this effect cancels out in the comparison procedure, the derived values for ΔH_f refer to 0 K.
- ¹⁸ B. Ruscic, *J. Chem. Phys.* **85**, 3776 (1986).
- ¹⁹ L. A. Curtiss, R. H. Nobes, J. A. Pople, and L. Radom, *J. Chem. Phys.* (submitted); also L. A. Curtiss and J. A. Pople (private communication).
- ²⁰ P. M. Guyon, W. A. Chupka, and J. Berkowitz, *J. Chem. Phys.* **64**, 1419 (1976).
- ²¹ C. E. Theodosiou, M. Inokuti, and S. T. Manson, *At. Data* **35**, 473 (1986).
- ²² F. Duschinsky, *Acta Physicochim. USSR* **8**, 551 (1937).
- ²³ This expression relates to equation (II, 200) in G. Herzberg, *Molecular Spectra and Molecular Structure II. Infrared and Raman Spectra of Polyatomic Molecules* (Van Nostrand, New York, 1945), p. 173.
- ²⁴ J. M. Dyke, N. B. H. Jonathan, A. Morris, and M. J. Winter, *Mol. Phys.* **39**, 629 (1980); J. M. Dyke, *J. Chem. Soc. Faraday Trans. II* **83**, 69 (1987).
- ²⁵ K. P. Huber and G. Herzberg, *Constants of Diatomic Molecules* (Van Nostrand, New York, 1979).
- ²⁶ S. G. Lias, J. E. Bartmess, J. F. Liebman, J. L. Holmes, R. D. Levin, and W. G. Mallard, *J. Phys. Chem. Ref. Data* **17**, Suppl. 1 (1988).
- ²⁷ Lias *et al.* (Ref. 26) cite $\Delta H_{f298}^{\circ}(\text{CH}_3\text{SH}) = -5.5 \pm 0.1$ kcal/mol (itself from another compilation) and derive $\Delta H_{f0}^{\circ}(\text{CH}_3\text{SH}) = -2.9$ kcal/mol. Starting from the same 298 K value, we arrive at $\Delta H_{f0}^{\circ}(\text{CH}_3\text{SH}) = -3.0 \pm 0.1$ kcal/mol, based on frequencies used in Ref. 11. This slightly lower value for $\Delta H_{f0}^{\circ}(\text{CH}_3\text{SH})$ was also consistently used throughout Ref. 1.
- ²⁸ J. M. Nicovich, K. D. Kreutter, C. A. van Dijk, and P. H. Wine, *J. Phys. Chem.* **96**, 2518 (1992); see also Ref. 1.
- ²⁹ S. G. Lias, J. F. Liebman, and R. D. Levin, *J. Phys. Chem. Ref. Data* **13**, 695 (1984).
- ³⁰ R. H. Nobes and L. Radom, *Chem. Phys. Lett.* **189**, 554 (1992).
- ³¹ P.A.₂₉₈ (CH₃SH) - P.A.₀ (CH₃SH) $\approx 1.5 \pm 0.3$ kcal/mol, based on a guesstimated ($H_{298}^{\circ} - H_0^{\circ}$) (CH₃SH⁺).
- ³² B. H. Solka and A. G. Harrison, *Int. J. Mass Spectrosc. Ion Phys.* **17**, 379 (1975).
- ³³ J. F. Wolf, R. H. Staley, I. Koppel, M. Taagepera, R. T. McIver, Jr., J. L. Beauchamp, and R. W. Taft, *J. Am. Chem. Soc.* **99**, 5417 (1977).
- ³⁴ $\Delta H_{f0}^{\circ}(\text{H}) = 51.634 \pm 0.001$ kcal/mol, $\Delta H_{f0}^{\circ}[\text{S}_{(g)}] = 65.66 \pm 0.06$ kcal/mol and $\Delta H_{f0}^{\circ}[\text{C}_{(g)}] = 169.98 \pm 0.11$ kcal/mol, from M. W. Chase, Jr., C. A. Davies, J. R. Downey, Jr., D. J. Frurip, R. A. McDonald, and A. N. Syverud, *J. Phys. Chem. Ref. Data* **14**, Suppl. 1 (1985).
- ³⁵ $\Delta H_{f0}^{\circ}(\text{CH}_3) = 35.78 \pm 0.12$ kcal/mol and $\Delta H_{f0}^{\circ}(\text{CH}) = 141.97 \pm 0.31$ kcal/mol, from V. P. Glushko, L. V. Gurvich, G. A. Bergman, I. V. Veits, V. A. Medvedev, G. A. Khachkuzov, and V. S. Yungman, *Termodinamicheskie Svoistva Individual'nykh Veshchestv*, Vol. 2 (Nauka, Moscow, 1979).
- ³⁶ $\Delta H_{f0}^{\circ}(\text{CH}_2) = 93.6 \pm 0.6$ kcal/mol, as adopted by R. K. Lengel and R. N. Zare, *J. Am. Chem. Soc.* **100**, 7495 (1978).
- ³⁷ $\Delta H_{f0}^{\circ}(\text{SH}) = 33.81 \pm 0.69$ kcal/mol, based on $D_0(\text{SH}) = 3.62 \pm 0.03$ eV from R. E. Continetti, B. A. Balko, and Y. T. Lee, *Chem. Phys. Lett.* **182**, 400 (1991).
- ³⁸ B. Ruscic and J. Berkowitz, *J. Chem. Phys.* **95**, 4033 (1991).
- ³⁹ K. M. A. Rafeey and W. A. Chupka, *J. Chem. Phys.* **48**, 5205 (1968).
- ⁴⁰ B. Ruscic and J. Berkowitz, *J. Chem. Phys.* **95**, 2416 (1991).